The effect of Static Chamber's Base on N_2O Flux in Drip Irrigation

Shahar Baram[1], Asher Bar-Tal[1], Alon Gal[1,2], Shmulik P. Friedman[1], David Russo[1]

[1]Institute for Soil, Water and Environmental Sciences, Agricultural Research Organization (ARO), Volcani Institute, 68 HaMacabim Rd. P.O Box 15159, Rishon Lezion 7505101, Israel
[2] The Mina and Everard Goodman Faculty of Life Sciences, Bar-Ilan University, Ramat Gan, Ramat-Gan 52900, Israel.

Correspondence to: Shahar Baram (sbaram@volcani.agri.gov.il)

Abstract

Static chambers are commonly used to provide *in-situ* quantification of N_2O fluxes. Despite their benefits, when left in the field, the physicochemical conditions inside the chamber's base may differ from the ambient, especially in drip-irrigated systems. This research aimed to study the effects of static chambers' bases on water and N-forms distribution and the impact it has on N_2O measurements in drip irrigation. N_2O emissions were measured in a drip-irrigated avocado orchard for two years, using bases with a dripper at their center (In) and bases installed adjacent to the dripper (adjacent). During the irrigation/fertigation season, the measured N_2O_{In} fluxes were greater than the $N_2O_{Adjacent}$ fluxes (0.82 ± 0.15 vs. 0.36 ± 0.05 ng cm^{-2} sec^{-1}). In contrast, during the winter, when the orchard is not irrigated or fertilized, insignificant differences were observed between the measured $N_2O_{Adjecent}$ and N_2O_{In} fluxes. Three dimentional simulations of water flow and N-forms transport and transformations showed two opposing phenomena (a) increased water contents, N concentrations, and downward flushing when the dripper is placed inside the base, and (b) hampering of the lateral distribution of water and solutes into the most bio-active part of the soil inside the base when the base is placed adjacent to the dripper. It also showed that both "In" and "adjacent" practices underestimate the "true" cumulative flux from a dripper with no base by ~25% and ~50%, respectively. A nomogram in a non-dimensional form corresponding to all soil textures, emitter spacings and discharge rates, was developed to determine the optimal diameter of an equivalent cylindrical base to be used along a single dripline.

1. Introduction

Static chambers are commonly used to provide *in-situ* quantification of N_2O fluxes from soil-plant systems (Clough et al., 2020). Ideally, such cambers should be as large as feasibly possible in order to capture spatial variation, where most chambers cover a surface area of $0.03 - 0.25$ m^{-2}. Commonly, static chambers are built from two separate parts: (i) bases (also known as collars or anchors) that are pushed into the ground, and (ii) chambers that are placed and sealed onto the bases during flux measurements.

It is acknowledged that static chambers suppress the gas concentration gradient at the soil-atmosphere interface. The magnitude of the chamber-induced errors is known to increase with increased chamber deployment time, decreased chamber height, greater soil air-filled porosity (Venterea, 2010). Different

methods have been developed to quantify/correct these errors (Venterea, 2010; Venterea et al., 2020). Proper use of static chambers calls for minimal disturbance of the soil surface and the prevention of lateral diffusion of N_2O beneath the bases' wall. To reduce perturbation of the soil structure, which can release pulses of gases, and to minimize the influence on the carbon and nitrogen turnover in the bases

40   (mainly the decaying process of cut roots) (Clough et al., 2020), bases are installed prior to the beginning of the experiment and left in the same location for the duration of the project. During installation, bases need to be inserted to at least the depth where N_2O concentrations are not being perturbed by feedback effects from the chamber (Rochette and Eriksen-Hamel, 2008; Healy et al., 1996; Hutchinson and Livingston, 2001). Despite their benefits, when bases are left in the field, atypical soil water contents,

45   aeration, temperature, and microbial processes may develop in them (Clough et al., 2020). Such perturbations must be minimized or avoided, especially in drip-fertigation systems where the localized concentrations of N and water content may increase the potential for N_2O emissions (Smart et al., 2011; Baram et al., 2018; Burton et al., 2008; Zebarth et al., 2008).

 A review of the published literature in which static chambers were used at drip-irrigated fields shows

50   inconsistency regarding the chamber's location relative to the emitter (dripper). In many studies, chamber's bases (i.e., metal or PVC frame) are installed adjacent to the drip lines to depths of 5 to 13 cm, prior to the beginning of the experiment and left in the same location for the duration of the project (Garland et al., 2014; Baram et al., 2018; Alsina et al., 2013; Verhoeven and Six, 2014; Tian et al., 2017; Scheer et al., 2008; Fentabil et al., 2016). An adidtional startegy is to install the bases to similar depths,

55   a day to few hours before sampling (Sanchez-Martín et al., 2010; Sánchez-Martín et al., 2008). Both strategies are applied to reduce perturbation of the soil structure following the base's insertion, as discussed above. In such practices, the base serves as a hydraulic barrier that prevents lateral movement of water from the dripper into the soil volume confined by it, especially close to the soil surface. Accordingly, the water-filled pore-space (WFPS; the ratio between the volumetric water content and the

60   porosity, also known as "water saturation degree", S) and the N-species concentrations in the base will most likely differ from the ambient ones. Sanchez-Martín et al. (2010), acknowledged these biases (especially in the water content) and, therefore, removed the bases after sampling, allowing lateral redistribution between sampling days. Wolff et al. (2017) and Vallejo et al. (2014) tried to overcome these limitations by installing the bases and sampling the fluxes directly after the fertigation event.

65   However, as mentioned before, such a sampling method could be affected by perturbation of the soil structure and root damage (Clough et al., 2020). Placement of drippers above the bases was also suggested as a way to minimize the differences between the soil water content and N concentrations inside the bases and that of the surroundings (Heller et al., 2010; Garland et al., 2014). Another suggestion was to split the dripper discharge into two separate drippers, one in the bases and the other outside

70   (Fentabil et al., 2016). Though these latter methods seem to overcome the base's disturbance of water and solute distribution in the topsoil, their actual impact on water and N-species distribution in the soil inside the base and their effect on the N_2O fluxes were never tested.

Many models have been developed to simulate N_2O emissions from soils. In all models, N_2O emission results mainly from nitrification and denitrification reactions, which in turn are affected by the following

75   parameters in the soil: (a) mineral N concentration [namely, nitrate (NO_3^-) and ammonium (NH_4^+)], (b) WFPS as a proxy for soil aeration and gas diffusion coefficient, (c) temperature, (d) pH, (e) redox potential, and (f) carbon availability (Rabot et al., 2015; Hénault et al., 2019; Wu and Zhang, 2014). This research aimed to study the effects of static chambers' bases on water and N-forms distribution inside it and the impact it has on N_2O emission measurements in drip irrigation. We used both field measurements

80   and three-dimensional (3-D) simulations of flow and transport in order to test the effect of the base diameter and its location relative to the dripper lateral on N_2O emissions.

2.   Materials and methods

2.1. Study site and N_2O measurements

N_2O fluxes were measured over a two-year period in a drip-irrigated avocado orchard. The orchard is

85   located near Kibbutz-Yasur in Western Galilee, Israel. The soil at the site is a Vertisol (58% clay dominated by montmorillonite) (Nemera et al., 2020). The climate at the site is Mediterranean, characterized by a relatively long dry season (April – October) requiring irrigation and a distinct rainy period during the winter (November – March). The trees are planted 3.5m apart on ridges (1.6m wide, 0.4m high), with 6m between rows. Each row of trees was irrigated with a set of two driplines (laterals),

90   located 0.9m apart along both sides of the trees, with 0.5m spaced 1.6 L h^{-1} drippers (UNIRAM, Netafim). From April through November, the orchard was fertigated every other day, using treated wastewater enriched with an ammonium sulfate nitrate solution (NH_4:NO_3 = 3:1), maintaining 50 – 70 mg-N L^{-1} in the fertigation solution.

From June 2018 through June 2020, N_2O fluxes were measured at mid-morning using

95   accumulation static chambers that were installed at 12 random locations in the avocado orchard. At each location, two chamber bases were inserted, one with a dripper at its center (In) and one adjacent to the dripper (adjacent) (Fig. 1). The bases were made from opaque polyvinylchloride (PVC) rings, 10 cm high and 19 cm internal diameter (ID, surface area of 283.5 cm^2). The rings were inserted to a depth of 6-8 cm two weeks prior to the start of the sampling campaign and remained in the soil for the duration of the

100 experiment. The chambers were built from a 20 cm sewer PVC cup (volume of 3119 cm^3), equipped with a vent (3 mm Swagelok bulkhead union with a 12 cm long coiled copper tube, 1.5 mm i.d.), covered with a bubble reflective foil and a rubber skirt to ensure sealing with the base. Fluxes were measured in real-time by circulating the headspace in the static gas chamber via Teflon tubes into a Fourier-transform infrared spectrometer (FTIR; Gasmet DX4000, Gasmet Technologies, Finland). During the enclosure

105 period, N_2O concentrations were recorded every five seconds, as an average average of 50 reads. N_2O fluxes (q) [g cm^{-2} sec^{-1}] were calculated based on the linear slope, representing the increase in N_2O concentration throughout 4 to 8 min enclosure time (Eq. 1). The Pearson's correlation coefficient (r^2) was calculated for the linearity of the slope, and readings were accepted when r^2 was >0.70.

[1]
$$q = \frac{dC_{gas}}{dt} * \frac{V_{chamber}}{A_{chamber}} * \frac{P}{RT} * M_w$$

where C_{gas} is the measured gas concentration [μL L^{-1}], t is the time [sec], $V_{chamber}$ [cm^3] and $A_{chamber}$ [cm^2] are the chamber volume and surface area respectively, P is the ambient pressure [atm], R is the gas law constant [0.08206 L atm mol^{-1} °K^{-1}], T is the temperature [°K], and M_w is the molecular weight of the gas [g mol^{-1}]. Daily values were obtained following the method of Parkin and Kaspar (2006), using a Q_{10} value of 3.72.

2.2. Modelling water flow, nutrients fate, and N₂O emissions

2.2.1. The physical domain and its parametrization

Employing a Cartesian coordinate system (x_1, x_2, x_3), where x_1 directed downwards, a subplot of the orchard consisting of a 3-D, spatially heterogeneous, variably saturated flow domain which extends over $L_1=2$m, $L_2=15$m, and $L_3=10$m along the x_1, x_2, and x_3 axes, respectively, is considered here. The subplot includes two adjacent tree rows, located 6m apart, with four trees, located 3.5m apart, along each row (Fig. SI-1)

Following Russo et al. (2020), the van Genuchten (1980) (VG) five-parameter model (*i.e.*, saturated conductivity, K_s, shape parameters, α and n, the saturated, θ_s, and residual, θ_r, values of water content, θ), was implemented here for the local description of the constitutive relationships for unsaturated flow. Based on previous studies (e.g., Russo et al., 1997; Russo and Bouton, 1992), it is assumed here that each of the VG parameters is a second-order stationary, statistically anisotropic, random space function, characterized by a constant mean, and a two-point covariance. Parameters of the latter, the variance and the correlation length-scales, were adopted from Russo and Bouton (1992). Grain-size distribution data was obtained by the laser diffraction method (Eshel et al., 2004) from 0.3m-segments of five soil cores extending to a depth of 1.2m. The data was used to estimate the local-scale VG parameters by an optimization procedure. For more details see Russo et al. (2020). Mean values of the VG parameters were estimated using the soil texture-based procedure suggested by Mishra et al. (1989). Details of the generation of the 3-D, cross-correlated realizations of the spatially heterogeneous VG parameters are given in Russo et al. (2006). Mean values and coefficients of variation (CV) of the resultant VG parameters are given in Table 1 of Russo et al. (2020). The numerical grid used for the generation of the 3-D VG parameters' field, was modified in order to account for the application of water by the drip irrigation system and for the geometry of the ridges. For more details, see Russo et al. (2020).

In addition, deterministic molecular diffusion coefficient for chloride (Cl$^-$), nitrate (NO₃$^-$) and ammonium (NH₄$^+$) in water, $D_0=5.4\cdot10^{-5}$ m^{2}d^{-1}, dimensionless Henry's constant for N₂O, $K_H=0.2$, and pore-scale dispersion tensor (with longitudinal dispersivity, $\lambda_L=2\times10^{-3}$m and transverse dispersivity, $\lambda_T=1\times10^{-4}$m (Perkins and Johnston, 1963), were considered in the simulations. First-order rate constants for nitrification and denitrification, K_1 and K_2, respectively, and liquid-solid partitioning coefficient for ammonium, K_{d1}, were taken into account as depth-dependent, implementing values within the range suggested by Lotse et al. (1992). Estimates of the root uptake coefficients for ammonium and nitrate, K_{u1} and K_{u2}, respectively, were calculated by extending the method of Nye and Tinker (1977); for more details see Russo et al. (2013). Root distribution data, adopted from Salgado and Cautin (2008), were employed in order to construct a time-invariant, normalized root depth-distribution function for the avocado trees.

2.2.2. Quantification of the flow and the transport

Considering water and nitrogen extraction by plant roots, water flow and solute (ammonium, nitrate, and chloride) transport in the 3-D, unsaturated, spatially heterogeneous flow system were simulated employing numerical solutions of the 3-D Richards equation and the 3-D single-region, advection-dispersion equation (ADE), respectively. Following Russo et al. (2015), the flow model was modified to account for irrigation by drippers. The iterative procedure described in Russo et al. (2006) was employed in order to determine the size of the time-dependent ponding area that may develop around the drippers at the soil surface during an irrigation event. Furthermore, following Russo et al. (2020), the sink term representing water uptake by the plant roots, which appears on the right-hand side of the Richards equation, was modified to account for the effect of the oxygen availability on water uptake. The maximization iterative (MI) approach proposed by Neuman et al. (1975) was adopted here in order to calculate water uptake by the plant roots and, concurrently, actual transpiration rate, $\tau_a(t)$.

Following Russo et al. (2013), the ADE was modified to account for nitrogen transformations and uptake by plants' roots in the soil-water-plant-atmosphere system. In addition, the competition between chloride and nitrate and its effect on the extraction of nitrogen by the plant roots, and the inhibition of nitrification induced by chloride were taken into account. For more details, see Russo and Kurtzman (2019). The uptake of nitrate and ammonium by the plants' roots was also calculated by a MI approach described by Eq. 6 in Russo et al. (2013).

N_2O emissions were calculated based on Hénault et al. (2005) and Hénault et al. (2019), accounting for nitrification and denitrification driven emissions. N_2O flux during denitrification (N_2O_{denit}; mg-N m^{-2} d^{-1}) was calculated as a combination of the potential denitrification rate (D_P; mg-N m^{-2} d^{-1}) and response functions to several environmental factors (Hénault et al. 2005):

Eq. 2
$$N_2O_{denit} = D_p \cdot F_w \cdot F_N \cdot F_T \cdot r_{max}$$

Where F_W is the denitrification response factor to the soil WFPS, assuming the WFPS parameter serves as a proxy of the oxygen availability for microorganisms (Supporting information (SI) Eq-SI1). F_N, is the denitrification response factor to soil nitrate content (dimensionless) (based on Michaelis–Menten saturation curve) (Eq-SI2), F_T is the denitrification response factor to soil temperature (Eq-SI3), r_{max} is the maximum ratio of N_2O to denitrified nitrate under anaerobic incubations (in this study $r_{max} = 0.3$) . N_2O production during nitrification (mg-N m^{-2} d^{-1}) was defined by Eq. 3 (Hénault et al. 2005):

Eq. 3
$$N_2O_{nit} = z\,N_A\,, \qquad WFPS < 0.62$$
$$N_2O_{nit} = r_{max} z\,N_A\,, \qquad WFPS \geq 0.62$$

Where z is the proportion of nitrified nitrogen emitted as N_2O (in this study $z = 0.006$), and N_A is the actual areal nitrification rate (mg-N m^{-2} d^{-1}).

Details of the flow and the transport equations and the numerical schemes employed to solve them are given elsewhere (Russo and Kurtzman, 2019; Russo et al., 2013).

2.2.3. Implementation

Meteorological data collected in the Yasur orchard were used to estimate the reference evapotranspiration, $ET_0(t)$, using Penman-Monteith method. Potential evapotranspiration rates, $\varepsilon_{tp}(t) = \varepsilon_p(t) + \tau_p(t)$ (where ε: evaporation, τ - transpiration), were estimated from the $ET_0(t)$ data using the time-

dependent crop coefficients actually used in the Yasur site. Assuming that the wetted soil surface area of the ridge is completely covered by the trees' canopy, a negligibly low soil evaporation rate was adopted for the surface area of the ridges, *i.e.*, $\tau_p(t)=\varepsilon\tau_p(t)$. For the soil surface area between the ridges outside the rooted zone, a negligibly small transpiration rate was assumed, *i.e.*, $\varepsilon_p(t)=\varepsilon\tau_p(t)$. Actual rates of water loss by evaporation, $\varepsilon_a(t)$, were implemented by a MI approach described in Russo et al. (2006).

The chamber base was modeled as a cuboid whose axes coincide with the coordinates of the flow system. The center of a given chamber base is located at a given, user-controlled point, $p=p(x_2,x_3)$, in the x_2x_3-horizontal plane; it extends vertically from the soil surface, $x_1=0$, to the depth of $x_1=Z_{bot}$, and horizontally from $x_{c21}=p-\delta x_2$ to $x_{c22}=p+\delta x_2$ and from $x_{c31}=p-\delta x_3$ to $x_{c32}=p+\delta x_3$, where $Z_{bot}=0.10m$ and $\delta x_2=\delta x_3$ vary between 0.1m to 0.2m. Unit-head-gradient is specified at $x_1=Z_{bot,}$ and no-flow is specified at $x_1=0$ and at the vertical planes of the chamber located at x_{c21} and x_{c22} and at x_{c31} and x_{c32}.

Appropriate initial conditions for the present analyses were created by considering measured water content and solutes' concentrations profiles obtained prior to the irrigation season. For the flow, a second-type upper boundary condition was imposed on the top boundary ($x_1=0$) with flux that is determined by the drippers' discharge and by the time-dependent potential soil evaporation flux. A unit-head-gradient-boundary was specified at the bottom boundary ($x_1=L_1$). For the transport, a first-type upper boundary condition was imposed on the top boundary with inlet concentrations corresponding to the irrigation water concentrations. A zero-gradient-boundary was specified at the bottom boundary. No-flow conditions are assumed for the vertical boundaries located at $x_2=0$, $x_2=L_2$, $x_3=0$, and $x_3=L_3$ (Fig. SI-1)

For a given location at the horizontal x_2x_3-plane and a given horizontal extent of the chamber base, starting at the beginning of the irrigation season (May 1st), flow and transport simulations proceeded for an irrigation period of 180d. Actual concentrations of nitrate and ammonium in the irrigation water (including amounts added as fertilizers) and concentration of chloride in the irrigation water used in the field experiments were implemented in the simulations.

2.3. Statistics

Data were analyzed using JMP® Pro Statistical Software version 15.0 (SAS Institute Inc., USA). For each base size or location, we used a t-test to analyze the effects of the base on the different variables. The data met the assumption of homogeneity of variances. Presented data are means ± standard error (SE), with *p* values (*p*) representing the level of statistical significance.

3. Results

3.1. Measured N₂O fluxes in the field

Results from two years of measuring showed that the N_2O fluxes were higher during the fertigation season (April through October) than during the winter period (November through March). During the winter, no significant differences were observed between the measured N_2O_{In} and $N_2O_{Adjacent}$ fluxes. In contrast, during the irrigation/fertigation season, the N_2O fluxes from the chambers with a dripper at their bases (N_2O_{In}) were on average 2.3±0.56 times greater than the fluxes from the chambers adjacent to the dripper ($N_2O_{Adjacent}$) (0.82 ± 0.15 vs. 0.36 ± 0.05) (Fig. 2). In 4.3% of the samples, $N_2O_{Adjacent}$ fluxes were

220   higher than the N_2O_{In} fluxes. This phenomenon only occurred when the measured fluxes were very low (<0.01 ng cm^{-2} sec^{-1}) in both locations and only following irrigation events and not fertigation events (Fig. 2). In 17% of the measurements, the N_2O_{In} and $N_2O_{Adjecent}$ fluxes differed by 20% or less (Fig. 2).

3.2. Simulation results

Simulation results show that during irrigation, the WFPS down the soil profile under the chamber's base

225   (20 cm ID), with a dripper at its center (WFPS$_{In}$), were higher than the WFPS under a normal representative dripper with no base (WFPS$_{No}$) (Fig. 3A and Fig. 4D). A day after the irrigation, the WFPS$_{In}$ decreased faster, leaving the soil profile under the WFPS$_{No}$ treatments wetter. Throughout the simulation period (i.e., from day five onwards), the WFPS at depths of 10, 20 and 30 cm hardly differ, and the WFPS$_{In}$ ranged from 0.77 to 0.63, while the WFPS$_{No}$ ranged from 0.74 to 0.65.

230   Ammonium-N (NH_4^+-N) concentrations in and under the chamber's base (NH_4^+-N$_{In}$) increased at all depths from ~5 mgL^{-1} at the start of the simulation to ~25 mgL^{-1} following 20 days. After 20 days, the concentrations remained high with minor changes. In contrast, the concentrations under a normal representative dripper with no base (NH_4^+-N$_{No}$) slightly increased during the 60 days of simulation (from 5 to 8 mgL^{-1}) (Fig. 3B). Unlike with the NH_4^+-N concentration, nitrate-N (NO_3^--N) concentrations

235   showed a clear oscillating trend over time that corresponded to the N concentration in the fertigation solution (Fig. 3C). The amplitude of change was higher when the dripper was placed inside the base.

Simulations with bases of variable sizes (i.e., no-base, 20, 30, and 40 cm ID) showed a clear size impact on the average NH_4^+-N and NO_3^--N concentrations in the top 10 cm of the soil (Fig. 5). For NO_3^--N, the smaller the base ID is, the higher the deviation from ambient (no-base) concentrations.

240   During fertigation events, NO_3^--N concentrations inside the 20, 30, and 40 cm bases increased by up to 212%, 159%, and 137%, respectively, relative to a dripper with no base around it. In contrast, between fertigation events, the concentrations decreased down to 10%, 32%, and 61% of the concentrations under a dripper with no base. Unlike the oscillating trend of NO_3^--N concentrations, NH_4^+-N concentrations during the simulated 60 days of fertigation gradually accumulated in the soil until they stabilized at

245   around 20 mg L^{-1}. The sharpest buildup was observed under the 20 and 30 cm ID bases where the NH_4^+-N concentrations were up to 300 times greater than the concentrations under a dripper with no-base (Figs. 5).

Simulated N_2O emissions showed a clear oscillating trend over time, which was affected by the irrigation and fertigation regime (Fig. 6). During fertigation events, N_2O fluxes from the 20 cm ID base

250   were on average higher by 14±6% ($p = 0.0345$) than the fluxes from a dripper with no base, with higher fluxes from deeper parts (< 10 cm) of the soil (Fig. 4C). However, the fluxes from the 30 and 40 cm ID bases were lower by 10±5% and 26±4%, respectively ($p < 0.001$, both). A day after a fertigation event, the fluxes from the 20, 30, and 40 cm ID chambers were -4±10%, -14±5%, and -26±3% lower than the fluxes from a dripper with no base ($p < 0.008$, all). More than one day after fertigation, the fluxes from

255   the 20, 30, and 40 cm ID chambers were significantly lower than from a dripper with no base, with the greatest reduction in the 20 cm ID base (-69±3%, -42±4%, and -24±3%). Irrigation events a day or two days following fertigations drastically reduced the N_2O fluxes, leading to fluxes that equaled 33±6%, 67±8%, and 85±5% of the fluxes measured from a dripper with no base.

Under a dripper with no-base and a 40 cm ID base, simulated N_2O emission was significantly
($p < 0.05$) affected by the simulated WFPS, NH_4^+-N, and NO_3^--N concentrations at depths of 10, 20, and
30 cm below the surface, with R^2 correlations of 0.10, 0.20 and 0.99, respectively (Table SI-2 and Table
SI-3). In contrast, under bases with a 20 and 30 cm ID, simulated N_2O emissions were significantly
affected only by the simulated NO_3^--N concentrations (Table SI-1, and Table SI-2, Table SI-3).

4. Discussion

Our field measurements show that $N_2O_{Adjecent}$ fluxes may be higher than the N_2O_{In} fluxes following
irrigation events or several days after fertigation events (Fig. 2). These values suggest either higher WFPS
or higher concentration of N in the base adjacent to the dripper. Simulation results show that the
differences in the WFPS between a base with a dripper at its center and between an undisturbed dipper
are in the range of ±4% following irrigations every other day (Fig 3A). It also shows that these differences
can be greater (±8%), especially at a depth of 30 cm, following sporadic irrigation events or irrigation
events at the start of the growing season (Fig 3A and Fig. 4D). Analysis of the simulations results shows
that the WFPS had a significant impact on the N_2O fluxes only when no base was used ($R^2<0.004$,
$p>0.598$ vs. $R^2<0.094$, $p<0.009$) (Table SI-3). Published literature shows that the WFPS-N_2O relation is
not always clear. N_2O emissions were thought to have their optimum in the range of 70–80% water-filled
pore space (WFPS) depending on soil type (Davidson et al., 2000). At higher soil water content, the
major end product of denitrification is N_2. Nevertheless, a comprehensive study of 51 soils across Europe
showed that most soils had their optimum N_2O emissions under WFPS wetter than 80% (Zechmeister-
Boltenstern et al., 2007). Similarly, Keller and Reiners (1994) found that N_2O emissions increased
exponentially with WFPS, even at WFPS greater than 80%. Bateman and Baggs (2005) showed that the
relative contribution of nitrification and denitrification to N_2O emission depended on the WFPS. Whereas
at 70% and 20% WFPS, most N_2O originated from denitrification, at 35–60% WFPS, nitrification was
the main process producing N_2O. Overall, the simulated WFPS indicated that the micropores in the soil
remained water-filled, which permits microbial activity without water stress, while the soil macropores
are air-filled, which permits relatively good aeration of the bulk of the soil, although anaerobic microsites
may exist. At such WFPS, both oxidative (nitrification) and reductive (denitrification) processes are
active in the soil.

It is well established that higher N concentrations lead to higher N_2O emissions (Wolff et al.,
2014, 2017; Baram et al., 2018; Schellenberg et al., 2012; Alsina et al., 2013; Butterbach-Bahl et al.,
2013). A clear indication of this phenomenon can be seen in Figures 3 and 4, the model's simulation of
water flow and NO_3^- and NH_4^+ transport in the subsurface. When the dripper is placed in the center of
the base, $NO_3^-_{In}$ concentrations in the top 30 cm may be 50 – 64 % higher during fertigation events and
up to 67% lower following irrigation or in the days following fertigation events. Inspection of the trend
over time shows that, on average, $NO_3^-_{In}$ concentrations are decreased by -19%±5% ($p = 0.017$) relative
to a dripper with no base. This phenomenon results from the higher WFPS and the geometry of the base
that limits lateral flow. As such, the water flow in the base is essentially 1D in the vertical direction,
which expedites downward water flow and N transport into the subsurface. NH_4^+, unlike NO_3^-, is

positively charged, hence readily adsorbs to the clays in the soil. Accordingly, $NH_4^+{}_{In}$ concentrations in the top 30 cm increased by 280% relative to a dripper with no base and remained higher throughout the season ($p < 0.001$) (Fig. 3).

300   Inspection of the correlations between the simulated N_2O fluxes and the NH_4^+ and NO_3^- concentrations show that N_2O emissions were mainly influenced by the NH_4^+ and NO_3^- concentrations (Table SI-2 and Table SI-3). These, in turn, were affected by the base's ID, with higher ID leading to less biases. It is known that N_2O emission fluxes vary from one fertilizer event to another, even at the same site with the same fertilizer type under similar environmental conditions (Cowan et al., 2020). Here we
305   show that an additional factor that must be accounted for is the location of the chamber's base relative to the water source and the perturbation that the base has on water and N-species distribution. Simulation results show that placing the dripper inside the base may increase the N_2O flux during a fertigation event by up to 52% relative to a dripper without a base. In tandem, N_2O fluxes following irrigation events or in the days following fertigation may be up to 91% lower when the dripper is placed inside the base (Fig.
310   7A). A similar effect is observed when the chamber's base is positioned adjacent to the dripper (i.e., up to 23% increase during fertigation and up to 97% decrease following irrigation events or in the days following fertigation). One should note that the modeled N_2O fluxes resulted mainly from denitrification, as suggested by Eq. 3 and its relation to the WFPS (Fig. 3A, Table SI-2, and Table SI-3). It is evident that under a different WFPS-N_2O_{nit} pattern, the base impact on the N_2O may increase in tandem with the
315   higher NH_4^+ concentrations. All of these results provide a good indication of the two opposing phenomena (a) increased WFPS, N concentrations and downward flushing when the dripper is placed inside the base, and (b) hampering of the lateral distribution of water and solutes into the most bio-active part of the soil inside the base when the base is placed adjacent to the dripper.

       Comparison of cumulative N_2O emission measured in 2018, 2019, and 2020 showed the N_2O_{In}
320   flux to be 50% – 60% higher than the $N_2O_{Adjecent}$ flux (98 – 120 mg m^{-2} vs. 60 – 74 mg m^{-2}). Simulation results showed similar differences between the two (N_2O_{In} ~68% higher, 9.53 vs. 6.48 mg N_2O-N m^{-2} over 60 days) (Fig. 7B). It also shows that both methods underestimate the "true" cumulative flux from a dripper with no base by ~25% and ~50%, respectively. These values suggest that in addition to measurement errors due to suppression of the gas concentration gradient at the soil-atmosphere in static
325   chambers (e.g., Venterea et al., 2020; Venterea, 2010), the impact of the camber's base on the water and N distribution provides an additional level of complexity, leading to an erroneous estimate of the true N_2O flux. Accordingly, the emission factors measured in such setups (e.g., Alsina et al., 2013; Baram et al., 2018; Fentabil et al., 2016; Garland et al., 2014; Scheer et al., 2008; Tian et al., 2017; Verhoeven and Six, 2014) are likely lower than the actual emission factors.

330   The degree to which the location of the chamber's base relative to the dripper affects the N_2O flux will depend on the soil properties and on the chamber's ID. Overall, an increase in the chamber's ID will decrease the abovementioned biases by reducing the lateral flow constraints posed by the chamber's base. An indication of this process can be seen in Figure 5 for the clayey soil used in this study. Such clayey soils have a large capillary length (i.e., tens of cm long), which supports high lateral capillary flow.
335   Accordingly, the use of a chamber with a larger ID (i.e., the simulated 40 cm or even larger) is required

to reduce the negative effects of the base on the water distribution near the surface and to provide a more reliable representation of the ambient fluxes around drippers.

A recommendation on the diameter of the chamber's base follows a simplified analysis of steady water flow from either a dripper (emitter) with no base (an undisturbed dripline) or a dripper surrounded by the cylindrical base (i.e., "In"). It is suggested to determine the diameter of the cylindrical base (d_{cyl}, cm), such that the water potential (or water content) at a chosen depth below the dripper (d_{ref}, cm) will be equal to that generated at the same depth below an undisturbed dripline with equally-spaced (d_{emit}, cm) drippers, depending on the soil capillary length (α^{-1}, cm). The matric flux potential in this location (φ_{ref}, cm^2 h^{-1}) is evaluated with analytical solutions to the linearized, steady water flow equation for a surface point source confined in a strip (its width equals d_{emit}), imitating an undisturbed single dripline, and for a surface point source in the center of a laterally-confined cylindrical domain, mimicking the dripper surrounded by the inserted-into-the-soil base wall (Eqs. [19] and [31] in Communar and Friedman (2011), respectively). The computations were performed using DIDAS (Friedman et al., (2016), https://app.agri.gov.il/didas/), firstly computing the φ_{ref} generated at depth d_{ref} under the undisturbed dripper and then determining d_{cyl} that will generate the same φ_{ref} at the same depth in an iterative, trial-and-error procedure.

The resulting reference water potential (Fig. 8A) and cylindrical base nomogram (Fig. 8B) are presented in a non-dimensional form corresponding to all soil textures and inter-emitter spacings and discharge rates (q, cm^3 h^{-1}), after normalizing all relevant lengths (d_{cyl}, d_{emit}, d_{ref}, cm), by the soil capillary length, (α^{-1}, cm), which describes the exponential decrease of the soil's hydraulic conductivity upon drying according to the Gardner's (1958) function, $K = K_s\exp(\alpha h)$ (K – hydraulic conductivity (cm h^{-1}), K_s – hydraulic conductivity at water-saturation (cm h^{-1}), h – pressure head (cm)), and reflects the dominance of capillarity over gravity forces in driving the water in partially-saturated soils. Coarse-textured, sandy soils are characterized with large α (cm^{-1}) values, and fine-textured, clayey soils with small ones.

The dimensionless matric flux potential ($\Phi_{ref} = 8\pi\varphi_{ref}/\alpha q$, $\varphi = K/\alpha$, or water content or pressure head (h) for a given soil (α) and dripper discharge rate (q)) decreases sharply with increasing distance between emitters (d_{emit}) or with coarsening (increasing α) of the soil texture, what counts is only their product αd_{emit}, and with increasing reference depth (αd_{ref}) below the emitter (Fig. 8A). At a dimensionless inter-emitter distance (αd_{emit}) of about 2, the Φ_{ref} (αd_{emit}) lines flatten as the effect of the neighboring emitters weakens and the potentials converge to those generated by a single emitter (not in a dripline, dash-dotted lines, Eq. [10] in Communar and Friedman (2010b)).

The upper limit of the dimensionless inter-emitter distance (αd_{emit}) in the depicted cylindrical base nomogram (Fig. 8B) is 2, as larger spacings are not recommended to assure overlap between the wetted bulbs (Communar and Friedman, 2010b), and a dimensionless reference depth of 1 (αd_{emit}) as the processes leading to N$_2$O emission are occurring at shallow depths. The diameter of the equivalent cylindrical base decreases sharply with increasing distance between emitters or for more sandy soils (αd_{emit}), the plotted ratio, d_{cyl}/d_{emit}, is approximately proportional to (αd_{emit})$^{-1/3}$. This is so because the relative (dimensionless) effect of the parallel strip walls (i.e., of the neigboring emitters) increases with

d_{emit}. However, the dependence of d_{cyl}/d_{emit} on the reference depth (αd_{ref}) is mild, a slight increase with depth of reference locations for small inter-emitter spacings (or for clayey soils), and virtually independence for large inter-emitter spacings (or for sandy soils). This is good news, as it means that an equivalent cylindrical base of chosen diameter can provide similar water contents at a range of depths below the dripper. The diameter of the equivalent cylindrical base is larger than the inter-emitter spacing ($d_{cyl}/d_{emit} > 1$) for smaller inter-emitter spacing, or for fine-texture soils, and slightly smaller than the inter-emitter spacing ($d_{cyl}/d_{emit} < 1$) for larger inter-emitter spacing, or for coarse-texture soils (Fig. 8B). As written above, intuitively, it is expected that since an infinitely-deep cylinder confines lateral water flow in all directions, while the symmetry vertical planes between drippers along the dripline confines it only in the direction of the dripline, d_{cyl} should be larger than d_{emit}. These results agree with the simualtion results discussed above, demonstrating mostly larger differences compared to undisturbed drippers for bases of smaller diametes (Figs.5 and 6). As a sensible inter-emitter spacing is about one capillary length, i.e., $\alpha d_{emit} = 1$, the recommended d_{cyl}/d_{emit} is about one (Fig. 8B), a base diameter equal to the inter-emitter spacing. Notice that the d_{cyl}/d_{emit} (αd_{emit}, αd_{ref}) nomogram is independent of the dripper discharge rate (q), since according to the linearized water flow equation used for the analysis (Eq. [5] in Communar and Friedman (2010), the matric flux potential generated by the drippers (point sources) is simply proportional to q, whatever is the geometry of the flow filed.

The use of the nomogram is very simple. Suppose we want to determine the diameter of a cylindrical base (d_{cyl}) that will optimally reproduce the wetting patterns under 50 cm-spaced drippers (d_{emit}) along a single dripline in a clayey soil with a capillary length (α^{-1}) of 100 cm, by requiring that the water potential (content) at a depth (d_{ref}) of 25 cm below the dripper will be the same. The dimensional emitter spacing (αd_{emit}) is thus 0.5, and the vertical arrow stops at the dimensionless reference depth (αd_{ref}) of 0.25 (black solid line in Fig. 8B), from which the horizontal arrow stretches to approximately $d_{cyl}/d_{emit} = 1.21$, i.e., the cylindrical base diameter should be larger by 21% compared to the inter-emitter spacing, about 60 cm. The soil capillary lengths (α^{-1}) of most agricultural soils vary between approximately 10 cm for sandy soils to 100 cm for structureless, clayey soils with common values of 20 to 40 cm for loams and fine sands (Friedman et al., 2016). If the value of the hydraulic conductivity at saturation is known, the soil capillary length can be evaluated with the universal relationship $\alpha = 0.04035 K_s^{1/2}$ (in which α is measured in cm^{-1} and K_s in cm h^{-1}) (Fig. 12 in Communar and Friedman (2010), also used in DIDAS).

The analysis used for constructing the $d_{cyl}/d_{emit}(\alpha d_{emit}$, $\alpha d_{ref})$ nomogram is based on addressing only water flow and applying multiple simplifying assumptions of steady flow, assuming an infinitely deep confining cylinder (as opposed to the just a few centimeters insertion of the chamber base, although the effect of 10cm insetion seems to affect the wetting patterns at large depths, Fig. 4D) and disregarding water uptake by plant roots and evaporation from the soil surface. Yet, it is believed that it provides plausible guidelines for choosing the optimal inserted-into-the-soil base diameter. In parallel, minimizing the depth to which bases are inserted to 1-2 cm will lower its impact on the water and N-species distribution inside it. This is especially true when short closure times are needed, such as when portable gas analyzers are used in the field. An alternative option is to develop a static chamber that does

not need a base. All of the above are crucial steps that are required to obtain accurate observations on
415   which small- and large-scale climate predication models are built.

5.   Conclusions

Based on two years of field measurements and numerical simulations of water flow, N-species transport
and reactions (i.e., nitrate and ammonium), and N_2O emissions, we conclude that the bases of static
chambers provide an underestimation of N_2O emissions when used in drip-irrigation. This is an outcome
420   of: (a) increased water contents, N concentrations, and downward flushing when the dripper is placed
inside the base, and (b) hampering of the lateral distribution of water and solutes into the most bio-active
part of the soil inside the base when the base is placed adjacent to the dripper. A nomogram is proposed
to determine the optimal diameter of a cylindrical base to be used along a single dripline. Further study
is suggested to determin the optimal insertion depth of bases based on the enclosure period. An alternative
425   option is to develop a static chamber that does not need a base.

6.   Author contribution

S. Baram and A. Bar-Tal supervised the project and acquired financial support. Baram designed the
experiments, analyzed the data, and wrote the manuscript with contributions from all co-authors. D.
Russo performed the detailed numerical simulations, and S. Friedman devised the equivalent cylinder
430   nomogram A. Gal collected the data in the feild.

7.   Acknowledgment

The study was funded by The Office of the Chief Scientist, Ministry of Agriculture and Rural
Development, Israel, Grant No.20-03-0027.

8.   References

435   Alsina, M. M., Fanton-Borges, A. C., and Smart, D. R.: Spatiotemporal variation of event related N_2O
and CH_4 emissions during fertigation in a California almond orchard, 4, art1,
https://doi.org/10.1890/ES12-00236.1, 2013.
Baram, S., Dabach, S., Jerszurki, D., Stockert, C. M., and Smart, D. R.: Upscaling point measurements
of N_2O emissions into the orchard scale under drip and microsprinkler irrigation, Agric. Ecosyst.
440   Environ., 265, 103–111, https://doi.org/10.1016/j.agee.2018.05.022, 2018.
Bateman, E. J. and Baggs, E. M.: Contributions of nitrification and denitrification to N_2O emissions
from soils at different water-filled pore space, Biol. Fertil. Soils, 41, 379–388,
https://doi.org/10.1007/s00374-005-0858-3, 2005.
Burton, D. L., Zebarth, B. J., Gillam, K. M., and MacLeod, J. A.: Effect of split application of fertilizer
445   nitrogen on N_2O emissions from potatoes, Can. J. Soil Sci., 88, 229–239,
https://doi.org/10.4141/CJSS06007, 2008.

Butterbach-Bahl, K., Baggs, E. M., Dannenmann, M., Kiese, R., and Zechmeister-Boltenstern, S.:
Nitrous oxide emissions from soils: how well do we understand the processes and their
controls?, Philos. Trans. R. Soc. Lond. B. Biol. Sci., 368, 20130122,
450   https://doi.org/10.1098/rstb.2013.0122, 2013.

Clough, T. J., Rochette, P., Thomas, S. M., Pihlatie, M., Christiansen, J. R., and Thorman, R. E.:
Global Research Alliance N_2O chamber methodology guidelines: Design considerations, J.
Environ. Qual., 49, 1081–1091, https://doi.org/https://doi.org/10.1002/jeq2.20117, 2020.

Communar, G. and Friedman, S. P.: Relative Water Uptake Rate as a Criterion for Trickle Irrigation
455   System Design: I. Coupled Source–Sink Steady Water Flow Model, Soil Sci. Soc. Am. J., 74,
1493–1508, https://doi.org/https://doi.org/10.2136/sssaj2009.0338, 2010a.

Communar, G. and Friedman, S. P.: Relative Water Uptake Rate as a Criterion for Trickle Irrigation
System Design: II. Surface Trickle Irrigation, Soil Sci. Soc. Am. J., 74, 1509–1517,
https://doi.org/https://doi.org/10.2136/sssaj2009.0339, 2010b.

460   Communar, G. and Friedman, S. P.: General Solution for Steady Infiltration and Water Uptake in Strip-
Shaped, Rectangular, and Cylindrical Domains, Soil Sci. Soc. Am. J., 75, 2085–2094,
https://doi.org/https://doi.org/10.2136/sssaj2011.0088, 2011.

Cowan, N., Levy, P., Maire, J., Coyle, M., Leeson, S. R., Famulari, D., Carozzi, M., Nemitz, E., and
Skiba, U.: An evaluation of four years of nitrous oxide fluxes after application of ammonium
465   nitrate and urea fertilisers measured using the eddy covariance method, Agric. For. Meteorol.,
280, 107812, https://doi.org/https://doi.org/10.1016/j.agrformet.2019.107812, 2020.

Davidson, E. A., Keller, M., Erickson, H. E., Verchot, L. V., and Veldkamp, E.: Testing a Conceptual
Model of Soil Emissions of Nitrous and Nitric Oxides Using two functions based on soil
nitrogen availability and soil water content, the hole-in-the-pipe model characterizes a large
470   fraction of the observed variation of nitric oxide and nitrous oxide emissions from soils,
Bioscience, 50, 667–680, https://doi.org/10.1641/0006-3568(2000)050[0667:tacmos]2.0.co;2,
2000.

Eshel, G., Levy, G. J., Mingelgrin, U., and Singer, M. J.: Critical Evaluation of the Use of Laser
Diffraction for Particle-Size Distribution Analysis, Soil Sci. Soc. Am. J., 68, 736–743,
475   https://doi.org/https://doi.org/10.2136/sssaj2004.7360, 2004.

Fentabil, M. M., Nichol, C. F., Jones, M. D., Neilsen, G. H., Neilsen, D., and Hannam, K. D.: Effect of
drip irrigation frequency, nitrogen rate and mulching on nitrous oxide emissions in a semi-arid
climate: An assessment across two years in an apple orchard, Agric. Ecosyst. Environ., 235,
242–252, 2016.

480   Friedman, S. P., Communar, G., and Gamliel, A.: DIDAS – User-friendly software package for
assisting drip irrigation design and scheduling, Comput. Electron. Agric., 120, 36–52,
https://doi.org/10.1016/J.COMPAG.2015.11.007, 2016.

Gardner, W. R.: Some steady-state solutions of the unsaturated moisture flow equation with application
to evaporation from a water table, Soil Sci., 4, 228–232, https://doi.org/10.1097/00010694-
485   195804000-00006, 1958.

Garland, G. M., Suddick, E., Burger, M., Horwath, W. R., and Six, J.: Direct N_2O emissions from a

Mediterranean vineyard: Event-related baseline measurements, Agric. Ecosyst. Environ., 195, 44–52, https://doi.org/https://doi.org/10.1016/j.agee.2014.05.018, 2014.

van Genuchten, M. T.: A Closed-form Equation for Predicting the Hydraulic Conductivity of
490   Unsaturated Soils, Soil Sci. Soc. Am. J, 44, 892–898, 1980.

Healy, R. W., Striegl, R. G., Russell, T. F., Hutchinson, G. L., and Livingston, G. P.: Numerical Evaluation of Static-Chamber Measurements of Soil—Atmosphere Gas Exchange: Identification of Physical Processes, Soil Sci. Soc. Am. J., 60, 740–747, https://doi.org/https://doi.org/10.2136/sssaj1996.03615995006000030009x, 1996.

495   Heller, H., Bar-Tal, A., Tamir, G., Bloom, P., Venterea, R. T., Chen, D., Zhang, Y., Clapp, C. E., and Fine, P.: Effects of Manure and Cultivation on Carbon Dioxide and Nitrous Oxide Emissions from a Corn Field under Mediterranean Conditions, J. Environ. Qual., 39, 437, https://doi.org/10.2134/jeq2009.0027, 2010.

Hénault, C. and Germon, J. C.: NEMIS, a predictive model of denitrification on the field scale, Eur. J.
500   Soil Sci., 51, 257–270, https://doi.org/https://doi.org/10.1046/j.1365-2389.2000.00314.x, 2000.

Hénault, C., Bourennane, H., Ayzac, A., Ratié, C., Saby, N. P. A., Cohan, J.-P., Eglin, T., and Gall, C. Le: Management of soil pH promotes nitrous oxide reduction and thus mitigates soil emissions of this greenhouse gas, Sci. Rep., 9, 20182, https://doi.org/10.1038/s41598-019-56694-3, 2019.

Hutchinson, G. L. and Livingston, G. P.: Vents and seals in non-steady-state chambers used for
505   measuring gas exchange between soil and the atmosphere, Eur. J. Soil Sci., 52, 675–682, https://doi.org/https://doi.org/10.1046/j.1365-2389.2001.00415.x, 2001.

Keller, M. and Reiners, W. A.: Soil-atmosphere exchange of nitrous oxide, nitric oxide, and methane under secondary succession of pasture to forest in the Atlantic lowlands of Costa Rica, Global Biogeochem. Cycles, 8, 399–409, https://doi.org/https://doi.org/10.1029/94GB01660, 1994.

510   Lotse, E. G., Jabro, J. D., Simmons, K. E., and Baker, D. E.: Simulation of nitrogen dynamics and leaching from arable soils, J. Contam. Hydrol., 10, 183–196, https://doi.org/https://doi.org/10.1016/0169-7722(92)90060-R, 1992.

Mishra, S., Parker, J. C., and Singhal, N.: Estimation of soil hydraulic properties and their uncertainty from particle size distribution data, J. Hydrol., 108, 1–18,
515   https://doi.org/https://doi.org/10.1016/0022-1694(89)90275-8, 1989.

Nemera, D. B., Bar-Tal, A., Levy, G. J., Lukyanov, V., Tarchitzky, J., Paudel, I., and Cohen, S.: Mitigating negative effects of long-term treated wastewater application via soil and irrigation manipulations: Sap flow and water relations of avocado trees (Persea americana Mill.), Agric. Water Manag., 237, 106178, https://doi.org/10.1016/j.agwat.2020.106178, 2020.

520   Neuman, S. P., Feddes, R. A., and Bresler, E.: Finite Element Analysis of Two-Dimensional Flow in Soils Considering Water Uptake by Roots: I. Theory, Soil Sci. Soc. Am. J., 39, 224–230, https://doi.org/https://doi.org/10.2136/sssaj1975.03615995003900020007x, 1975.

Nye, P. and Tinker, P. B.: Solute Movement in the Soil-Root System, Blackwell Scientific Publications: Hoboken, NJ, USA, 342 pp., 1977.

525   Parkin, T. B. and Kaspar, T. C.: Nitrous oxide emissions from corn-soybean systems in the midwest., J. Environ. Qual., 35 4, 1496–1506, 2006.

Perkins, T. K. and Johnston, O. C.: A Review of Diffusion and Dispersion in Porous Media, Soc. Pet. Eng. J., 3, 70–84, https://doi.org/10.2118/480-PA, 1963.

Rabot, E., Cousin, I., and Hénault, C.: A modeling approach of the relationship between nitrous oxide
530   fluxes from soils and the water-filled pore space, Biogeochemistry, 122, 395–408, https://doi.org/10.1007/s10533-014-0048-1, 2015.

Rochette, P. and Eriksen-Hamel, N. S.: Chamber Measurements of Soil Nitrous Oxide Flux: Are Absolute Values Reliable?, Soil Sci. Soc. Am. J., 72, 331–342, https://doi.org/https://doi.org/10.2136/sssaj2007.0215, 2008.

535   Russo, D. and Bouton, M.: Statistical analysis of spatial variability in unsaturated flow parameters, Water Resour. Res., 28, 1911–1925, https://doi.org/https://doi.org/10.1029/92WR00669, 1992.

Russo, D. and Kurtzman, D.: Using Desalinated Water for Irrigation: Its Effect on Field Scale Water Flow and Contaminant Transport under Cropped Conditions, 11, 687, https://doi.org/https://doi.org/10.3390/w11040687, 2019.

540   Russo, D., Russo, I., and Laufer, A.: On the spatial variability of parameters of the unsaturated hydraulic conductivity, Water Resour. Res., 33, 947–956, https://doi.org/https://doi.org/10.1029/96WR03947, 1997.

Russo, D., Zaidel, J., Fiori, A., and Laufer, A.: Numerical analysis of flow and transport from a multiple-source system in a partially saturated heterogeneous soil under cropped conditions,
545   Water Resour. Res., 42, https://doi.org/https://doi.org/10.1029/2006WR004923, 2006.

Russo, D., Laufer, A., Shapira, R. H., and Kurtzman, D.: Assessment of solute fluxes beneath an orchard irrigated with treated sewage water: A numerical study, Water Resour. Res., 49, 657–674, https://doi.org/10.1002/wrcr.20085, 2013.

Russo, D., Laufer, A., Bardhan, G., and Levy, G. J.: Salinity control in a clay soil beneath an orchard
550   irrigated with treated waste water in the presence of a high water table: A numerical study, J. Hydrol., 531, 198–213, https://doi.org/https://doi.org/10.1016/j.jhydrol.2015.04.013, 2015.

Russo, D., Laufer, A., and Bar-Tal, A.: Improving water uptake by trees planted on a clayey soil and irrigated with low-quality water by various management means: A numerical study, Agric. Water Manag., 229, 105891, https://doi.org/https://doi.org/10.1016/j.agwat.2019.105891, 2020.

555   Salgado, E. and Cautin, R.: Avocado root distribution in fine and coarse-textured soils under drip and microsprinkler irrigation, Agric. Water Manag., 95, 817–824, 2008.

Sanchez-Martín, L., Meijide, A., Garcia-Torres, L., and Vallejo, A.: Combination of drip irrigation and organic fertilizer for mitigating emissions of nitrogen oxides in semiarid climate, Agric. Ecosyst. Environ., 137, 99–107, https://doi.org/https://doi.org/10.1016/j.agee.2010.01.006,
560   2010.

Sánchez-Martín, L., Arce, A., Benito, A., Garcia-Torres, L., and Vallejo, A.: Influence of drip and furrow irrigation systems on nitrogen oxide emissions from a horticultural crop, Soil Biol. Biochem., 40, 1698–1706, https://doi.org/https://doi.org/10.1016/j.soilbio.2008.02.005, 2008.

Scheer, C., Wassmann, R., Kienzler, K., Ibragimov, N., and Eschanov, R.: Nitrous oxide emissions
565   from fertilized, irrigated cotton (Gossypium hirsutum L.) in the Aral Sea Basin, Uzbekistan: Influence of nitrogen applications and irrigation practices, Soil Biol. Biochem., 40, 290–301,

https://doi.org/10.1016/J.SOILBIO.2007.08.007, 2008.

Schellenberg, D. L., Alsina, M. M., Muhammad, S., Stockert, C. M., Wolff, M. W., Sanden, B. L.,
Brown, P. H., and Smart, D. R.: Yield-scaled global warming potential from N$_2$O emissions and
570 CH4 oxidation for almond (Prunus dulcis) irrigated with nitrogen fertilizers on arid land, Agric.
Ecosyst. Environ., 155, 7–15, 2012.

Smart, D. R., Alsina, M. M., Wolff, M. W., Matiasek, M. G., Schellenberg, D. L., Edstrom, J. P.,
Brown, P. H., and Scow, K. M.: N$_2$O Emissions and Water Management in California Perennial
Crops, in: Understanding Greenhouse Gas Emissions from Agricultural Management, edited by:
575 Guo, L., Gunasekara, A., and McConnell, L., ACS Symposium Series; American Chemical
Society:, Washington, DC, 227–255, 2011.

Tian, D., Zhang, Y., Mu, Y., Zhou, Y., Zhang, C., and Liu, J.: The effect of drip irrigation and drip
fertigation on N$_2$O and NO emissions, water saving and grain yields in a maize field in the
North China Plain, Sci. Total Environ., 575, 1034–1040,
580 https://doi.org/https://doi.org/10.1016/j.scitotenv.2016.09.166, 2017.

Vallejo, A., Meijide, A., Boeckx, P., Arce, A., García-torres, L., Aguado, P. L., and Sanchez-martin,
L.: Nitrous oxide and methane emissions from a surface drip-irrigated system combined with
fertilizer management, Eur. J. Soil Sci., 65, 386–395, https://doi.org/10.1111/ejss.12140, 2014.

Venterea, R. T., Petersen, S. O., de Klein, C. A. M., Pedersen, A. R., Noble, A. D. L., Rees, R. M.,
585 Gamble, J. D., and Parkin, T. B.: Global Research Alliance N$_2$O chamber methodology
guidelines: Flux calculations, J. Environ. Qual., 49, 1141–1155,
https://doi.org/https://doi.org/10.1002/jeq2.20118, 2020.

Venterea, R. T. V. A.-R. T.: Simplified Method for Quantifying Theoretical Underestimation of
Chamber-Based Trace Gas Fluxes, J. Environ. Qual., 39, 126–135,
590 https://doi.org/10.2134/jeq2009.0231, 2010.

Verhoeven, E. and Six, J.: Biochar does not mitigate field-scale N$_2$O emissions in a Northern California
vineyard: An assessment across two years, Agric. Ecosyst. Environ., 191, 27–38,
https://doi.org/https://doi.org/10.1016/j.agee.2014.03.008, 2014.

Wolff, M. W., Schellenberg, D. L., Sanden, B. L., Brown, P. H., and Smart, D. R.: Reducing Reactive-
595 N Loss from Fertigation: High-Frequency Application and Fertilizer Selection, in: Poster
presented at the annual meeting of the Almond Board of California. Sacramento, California,
USA, 2014.

Wolff, M. W., Hopmans, J. W., Stockert, C. M., Burger, M., Sanden, B. L., and Smart, D. R.: Effects
of drip fertigation frequency and N-source on soil N$_2$O production in almonds, Agric. Ecosyst.
600 Environ., 67–77, 2017.

Wu, X. and Zhang, A.: Comparison of three models for simulating N$_2$O emissions from paddy fields
under water-saving irrigation, Atmos. Environ., 98, 500–509,
https://doi.org/https://doi.org/10.1016/j.atmosenv.2014.09.029, 2014.

Zebarth, B. J., Rochette, P., Burton, D. L., and Price, M.: Effect of fertilizer nitrogen management on
605 N$_2$O emissions in commercial corn fields, Can. J. Soil Sci., 88, 189–195,
https://doi.org/10.4141/CJSS06010, 2008.

Zechmeister-Boltenstern, S., Schaufler, G., and Kitzler, B.: NO_2, N_2O, CO_2 and CH_4 fluxes from soils under different land use: temperature sensitivity and effects of soil moisture, Geophys. Res. Abstr., 8, 7968, 2007.

610

9. Figures
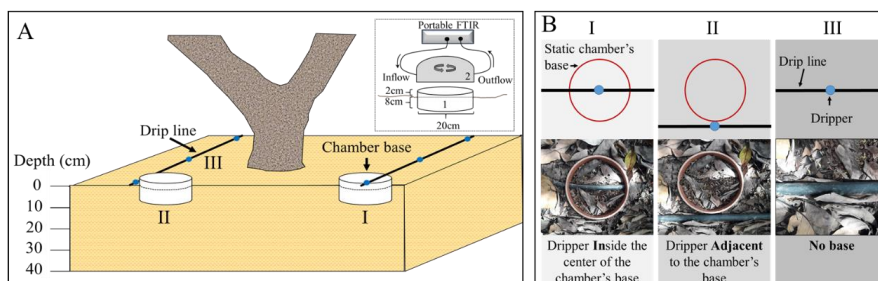
Figure 1. Schematic side view (A) and top view (B) representation of the static chamber setup used to
615   measure N$_2$O fluxes in an Avocado orchard and their locations (I, II, III) relative to the drip line and the
drippers.
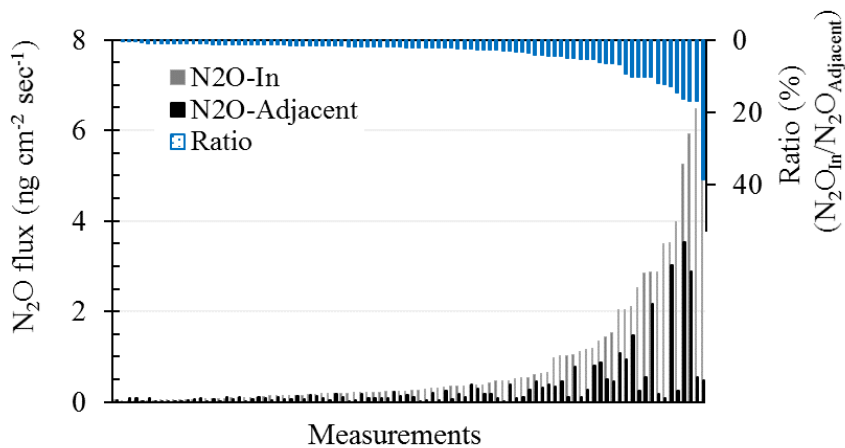
Figure 2. N$_2$O fluxes measured in static chambers with a dripper in their base (N$_2$O$_{In}$) and in static
chambers with a dripper adjacent to their base (N$_2$O$_{Adjacent}$), and the ratio between N$_2$O$_{In}$ and N$_2$O$_{Adjacent}$
620   at each one of the 12 sampling locations at all sampling days.
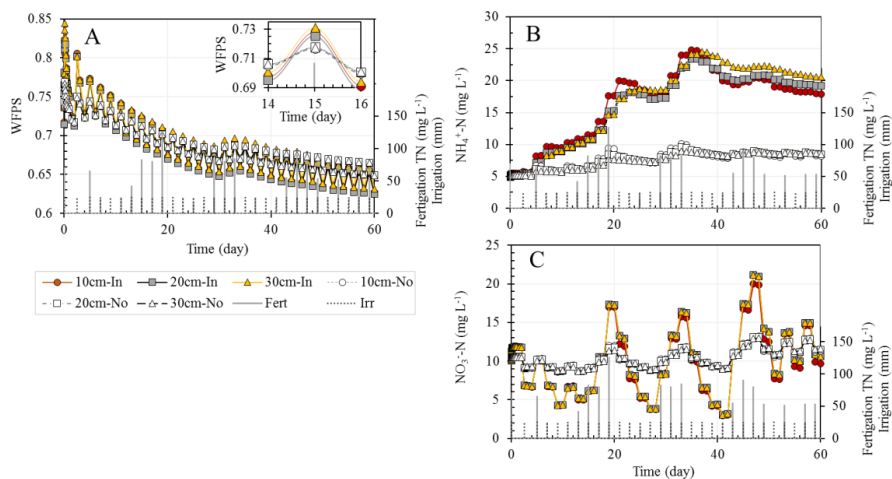
Figure 3. Simulation results of the change over time in (A) water filled pore space (WFPS), (B) NO_3^--N and (C) NH_4^+-N concentrations at three depths (10, 20 and 30 cm) under a base of a static chambers, with a dripper at its center (filled shapes – In), and under a dripper without a base (light empty shapes – No) following irrigation every other day, and fertigation events. The top right corner of (A) shows a zoom in on the WFPS cycle during three consecutive days: the day after fertigation (day 14), the day of fertigation (day 15) and the day following the fertigation event (day 16). Total nitrogen (TN) concentration in the fertigation solution is the sum of NO_3^--N and NH_4^+-N concentrations.
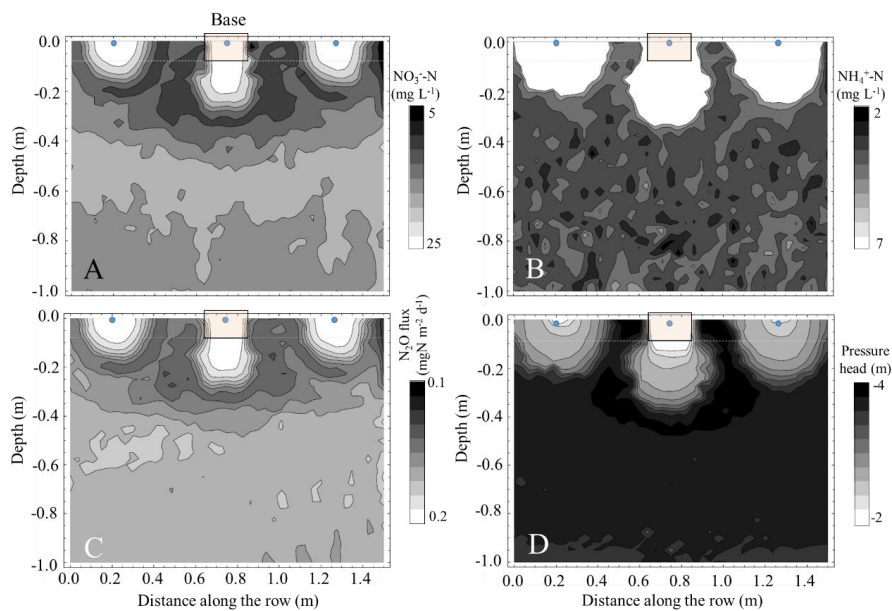
630

Figure 4. Contours of the simulated (A) nitrate-N (NO$_3^-$-N) and (B) ammonium-N (NH$_4^+$-N) concentrations, (C) vertical N$_2$O flux (positive upwards) and (D) pressure head distributions in the vertical x$_1$x$_3$-plane of the flow domain in the vicinity of one of the drippe line laterals along one of the ridges whose center is located at x$_2$=5.1m (Fig. SI-1). The figure shows three adjacent drippers, where the center dripper is confined by a static chamber's base. The presented data is a snapshot following 30 days of fertigation.

635
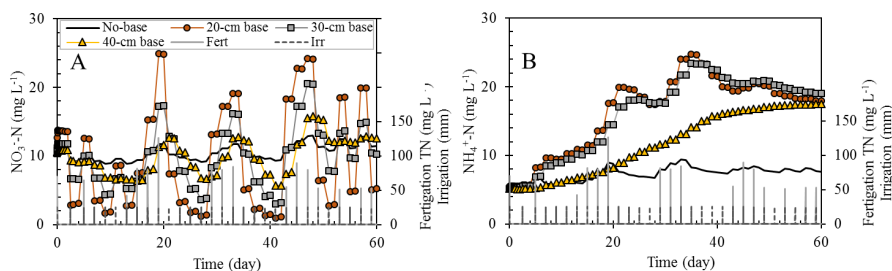
Figure 5. Simulation results of the change over time in NO_3^--N and NH_4^+-N concentrations in the top
640   soil (0 – 10cm) under bases of variable sizes (i.e., no-base, 20, 30, and 40 cm internal diameter) with a
dripper at their centers. Total nitrogen (TN) concentration in the fertigation solution is the sum of NO_3^--
N and NH_4^+-N concentrations.

Figure 6. Simulation results of the change over time in N_2O-N fluxes (A) at 10, 20 and 30cm below a
645   base with a dripper at its center (In) and under a dripper without a base (No), and (B) in the topsoil (0 –
10cm) under bases of variable sizes (i.e., no-base, 20, 30, and 40 cm internal diameter) with a dripper at
their centers. Total nitrogen (TN) concentration in the fertigation solution is the sum of NO_3^--N and
NH_4^+-N concentrations.

650
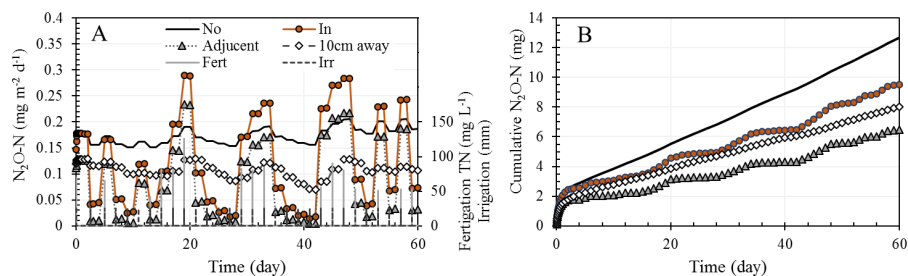
Figure 7. Simulation results of (A) daily and (B) cumulative N_2O-N emissions from the soil surface
under (No) and 10 cm away from a dripper without a chamber base, from a chamber base with a dripper
at its center (In) and a base adjacent to the dripper (adjacent), during consecutive fertigation events over
a period of 60 days.

655
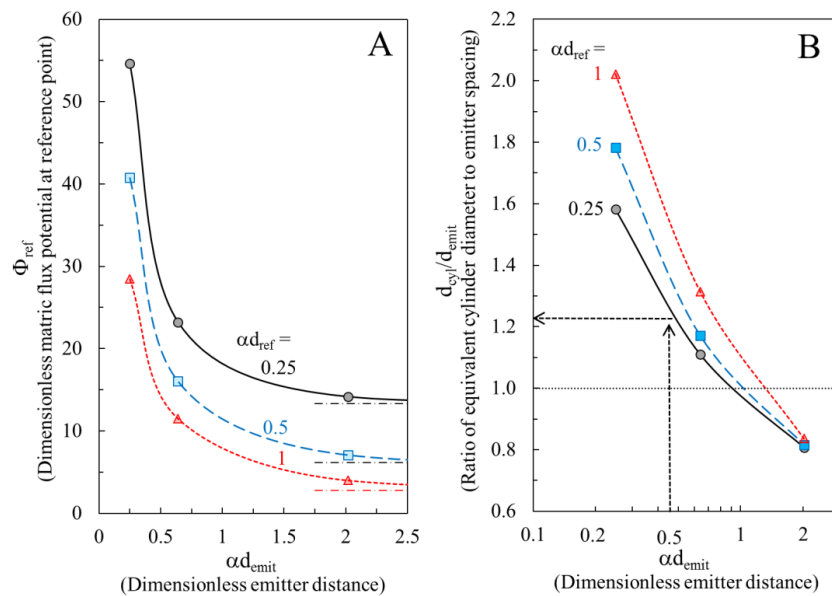
Figure 8. (A) Non-dimensional matric flux potential (Φ_{ref}), and (B) the ratio between the equivalent cylindrical base diameter (d_{cyl}) and the emitter spacing (d_{emit}), as a function of the non-dimensional distance between emitters (αd_{emit}), for different non-dimensional depths (αd_{ref}) below the emitter. The
660   dash-dotted lines on (A) represent Φ_{ref} at the given depth below a single emitter. $\Phi_{ref} = 8\pi\varphi_{ref}/\alpha q$, α is the soil's capillary lengths, q is the emitter discharge rate.